Supplementary Information for "Emergence of Chern Insulating States in Non-Magic Angle Twisted Bilayer Grapheme"

Cheng Shen(沈成)[1,2], Jianghua Ying(应江华)[1,2], Le Liu(刘乐)[1,2], Jianpeng Liu(刘健鹏)[3,4], Na Li(李娜)[1,2,6], Shuopei Wang(王硕培)[1,2,6], Jian Tang(汤建)[1,2], Yanchong Zhao(赵岩翀)[1,2], Yanbang Chu(褚衍邦)[1,2], Kenji Watanabe[7], Takashi Taniguchi[8], Rong Yang(杨蓉)[1,5,6], Dongxia Shi(时东霞)[1,2,5], Fanming Qu(屈凡明)[1,2,6], Li Lu(吕力)[1,2,6], Wei Yang(杨威)[1,2,6*], and Guangyu Zhang(张广宇)[1,2,5,6*]

[1]*Beijing National Laboratory for Condensed Matter Physics; Key Laboratory for Nanoscale Physics and Devices, Institute of Physics, Chinese Academy of Sciences, Beijing 100190, China*

[2]*School of Physical Sciences, University of Chinese Academy of Sciences, Beijing 100190, China*

[3]*School of Physical Sciences and Technology, ShanghaiTech University, Shanghai 200031, China*

[4]*ShanghaiTech laboratory for topological physics, ShanghaiTech University, Shanghai 200031, China*

[5]*Beijing Key Laboratory for Nanomaterials and Nanodevices, Beijing 100190, China*

[6]*Songshan-Lake Materials Laboratory, Dongguan, Guangdong523808, China*

[7] *Research Center for Functional Materials, National Institute for Materials Science, 1-1 Namiki, Tsukuba 305-0044, Japan*

[8]*International Center for Materials Nanoarchitectonics, National Institute for Materials Science, 1-1 Namiki, Tsukuba 305-0044, Japan*

[*]Corresponding author: wei.yang@iphy.ac.cn; gyzhang@iphy.ac.cn

1. Device fabrication, twist angle distribution and band gap at CNP

The hBN/TBG/hBN sandwich structure is fabricated through a typical "tear and stack" method[1] and then followed by ebeam lithography and reactive ion etching techniques. One-dimensional Cr/Au edge contact is applied[2]. We misalign graphene and hBN substrate to preserve C_2 symmetry, and also reserve untwisted monolayer graphene where we can check whether the C_2 symmetry is truly kept according to its transport behavior. An absence of satellite resistance peaks in the measured density range for monolayer graphene reveals little moiré superlattice potential modulation present between graphene and hBN (Fig. S1b).

We extract roughly the dominant twist angle between each Hall bar pairs by the formula $n_s = \frac{8\theta^2}{\sqrt{3}a^2}$, which relates the twist angle θ to carrier density n_s of full filling (here a is the graphene lattice constant). A further analysis of Hofstadter butterfly features, for instance Brown-Zak oscillations and fractal minibands, which directly give moiré unit cell area A according to $\phi = BA = \phi_0/q$ (here ϕ is the featured rational magnetic flux, q is an integer, and B is the corresponding magnetic field), finally help us to define the exact value of twist angles. For 1.25 degree device, we extracted the twist angle from the carrier densities at which C=-3, -2, -1 Chern insulators at B=0T. And for 1.38 degree device, the twist angle is extracted from the Brown-Zak

oscillations of Hofstadter butterfly due to the rational filling of magnetic flux in a moiré unit cell to quantum flux. For 1.43 degree device, the twist angle is quantified from carrier density difference between two points at B=0T where two set of landau levels fan out.

Fig. S1c shows temperature-varied resistance behavior in TBG with θ=1.25°. A metal-insulator transition occurs at low temperature, indicating gap opening at CNP. The linearly fitted thermal activation gap is about 1.35meV. Gap opening at CNP is typically attributed to C_2T symmetry breaking[3], which is specifically induced by a C_2 symmetry or T symmetry breaking. As C_2 symmetry is most likely already kept in our device, we thus speculate incipient T symmetry breaking present in our device.

We summarize the transfer curves for all pairs of probes on both sides of the hall bar in Fig. S2. For probe pairs 2-3 and 10-9, which are located at different sides but a same distance from probe 1, they show similar carrier density for fulfilling, i.e. the similar twist angle, yet with different twist inhomogeneity ($\pm$ 0.03° for 2-3 and $\pm$0.08° for 10-9). Results are the same for probes 3-4 and 9-8, as well as 4-5 and 8-7, with a moderate twist angle of ~$\pm$0.03°. The twist angle is increased when probes are further away from probe 1. In fact, such a twist angle distribution is most likely caused by the presence of bubbles at probes 1 and 6, which produce twist angle gradient from 1 to 6. Our transport data thus show an average result over a specific twist angle range. Despite the moderate twist angle inhomogeneity, it is noted that we can extract the exact twist angle contributed to the transport data precisely from the magnetic flux ϕ_0/q for Brown-Zak oscillation and carrier density at which Chern insulators are traced to at B=0T.

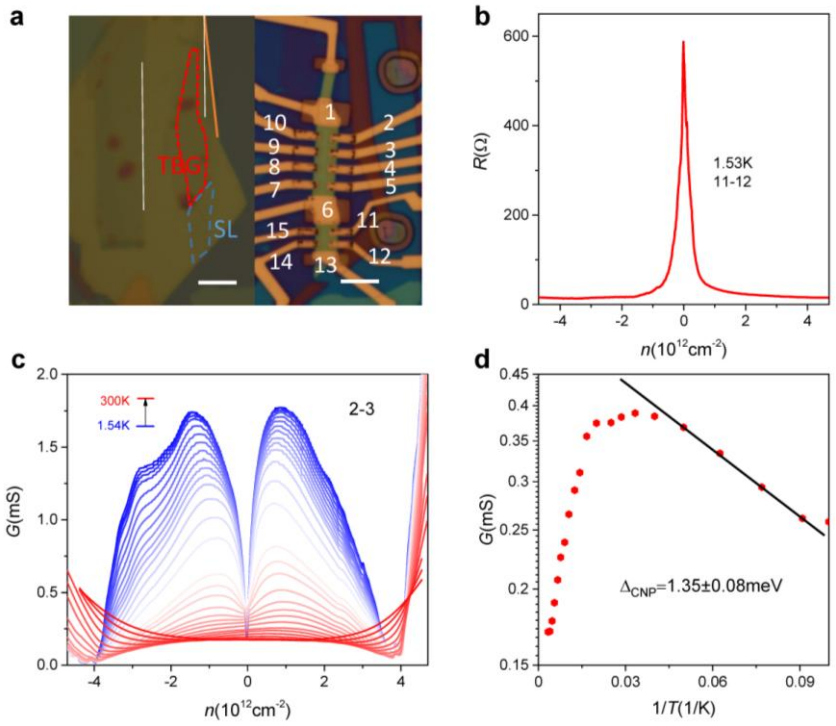

FIG.S1 Symmetry breaking in TBG device. a, optical microscope images of our device. The left one shows initial sandwich image. We outline the edge direction of hBN and graphene with orange and white lines, respectively. Red and blue dash lines enclose regions of TBG and monolayer graphene, respectively. Scale bars of both images represent 4μm. b, four-terminal resistance as a function of carrier density in monolayer graphene. c, temperature dependence of four-terminal conductance acquired between electrode 2 and 3. d, Arrhenius fitting of thermal activation gap at CNP.

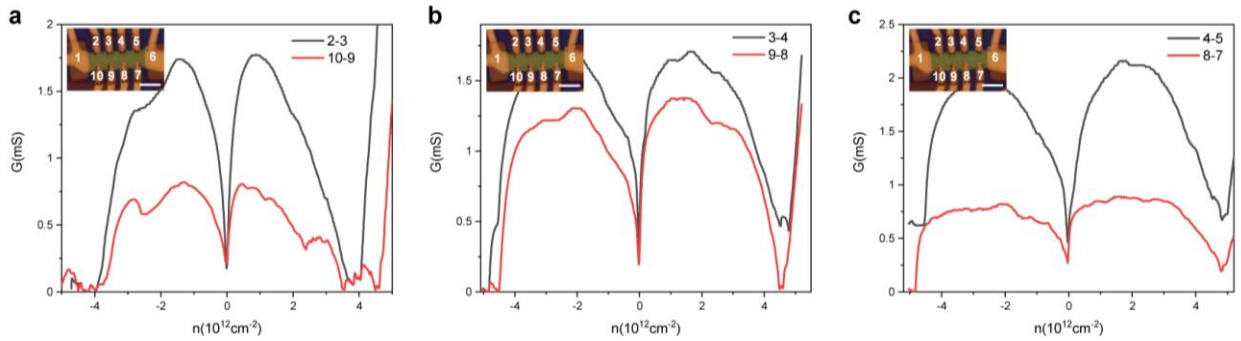

FIG.S2 Twist angle distribution all over the device. From the carrier density where gap edge appears for fulfilling, we extract the twist angle these probes as ~1.25 °(a), ~1.38 °(b) and 1.43 °(c). The data are acquired at 1.7K.

Generally speaking, mixed twist angle or twist angle inhomogeneity will tend to broaden the resistance peak at full filling, or even yield several peaks and thus bring several set of landau levels in the fan diagram (noted that the presence of gap opening at full filling will also tend to increase the width of the resistance peak). In our transport data, we only see two set of landau level, one from the charge neutral point, and the other from moiré superlattice period, which suggests trivial role played by twist angle inhomogeneity and a good sample quality of our device.

Besides, mixed twisted angle may bring additional scattering in the TBG and make it difficult to observe well quantized hall conductance plateau. However, the failure to observe quantized conductance in our 1.25 degree device is more likely due to big bandwidth at non-optimum twist angle, rather than few meV at magic angle of ~1.1 degree.

Lastly, mixed twisted angle is also predicted to induce C_3 symmetry breaking and lift landau level degeneracy in TBG devices[4]. This might relate to the lifted degeneracy transition from 8 folds to 4 folds for Landau levels emanating from charge neutral point, indicated by the dashed line in the figure below. However, electron interaction might also lift the degeneracy of landau levels.

2. Emergence of symmetry-broken and fractional Landau levels in remote bands

While most of attention is focused on the flat band in TBG, characteristics of remote dispersive bands are rarely studied. For remote bands, Fermi surface encloses Γ point in moiré Brillouin zone, producing four-fold spin-valley degeneracy. We find here that the four-fold degeneracy is fully lifted, yielding well-developed symmetry-broken LLs with ν_{LL}=1, 2, 3 (Fig. S3). These LLs are characterized by longitudinal magnetoresistance R_{xx} minima around zero, but without Hall plateaus due to twist angle inhomogeneity. We further find two R_{xx} minima trajectories with a slope $\frac{dB}{dn} = \frac{\phi_0}{\nu_{LL}}$, where ν_{LL} for one LL is estimated to be 1/3, and another uncertainly to be 2/3 or 3/5. This phenomenon indicates an emergence of fractional quantum Hall effect (FQHE) for remote bands.

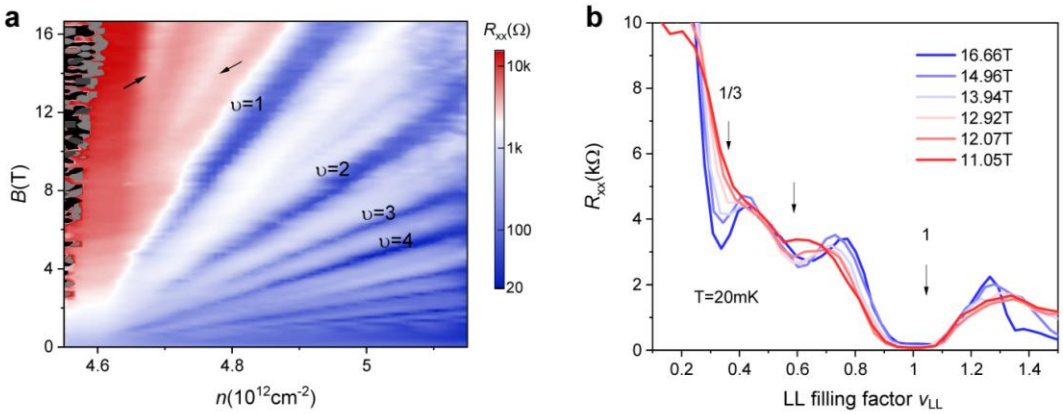

FIG.S3 Symmetry-broken Landau levels and signatures of fractional quantum Hall effects in remote dispersive bands in θ=1.25 ° TBG. The arrows in (a) point to R_{xx} minima of fractional Landau levels, as depicted in (b).

3. Chern insulators: gap size, Hall resistance and onset at tiny field

Because of the pronounced twist angle inhomogeneity in our device, Hall resistances for Chern insulators (Fig. S5) deviate from quantized plateaus, instead shows a peak tracing the corresponding R_{xx} minima as in Fig. 2a. We apply Arrhenius fitting to obtain the thermal activation gap for Chern insulator (-2, -2). At B=9T, its gap reaches to 11.7K, which is comparable to that of LL with ν_{LL}=-2 from CNP. We also zoomed in the LL fan diagram to focus on the onset of Chern insulator (-2, -2). Fig. S6 shows that the R_{xx} minima and also sign change of dR_{xx}/dn for Chern insulator (-2, -2) develop below B=1T.

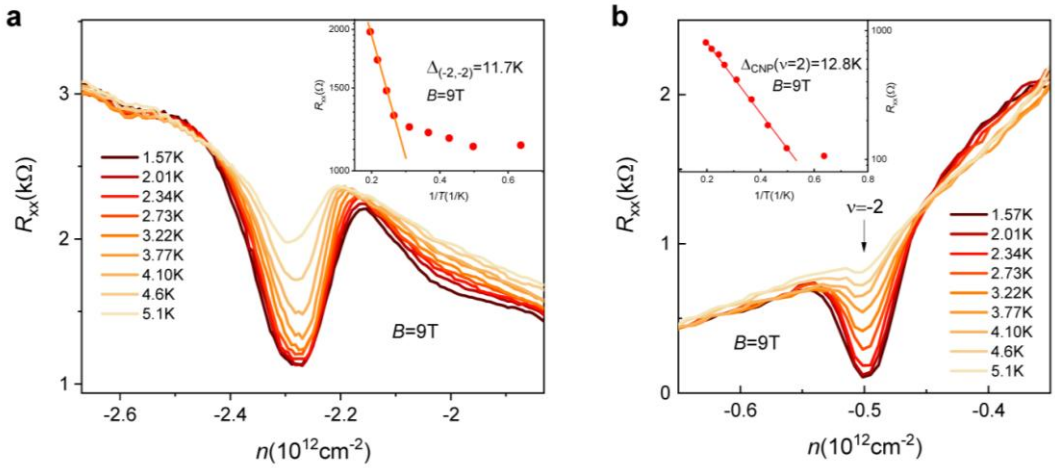

FIG.S4 Temperature dependence of R_{xx} at B=9T for Chern insulator (-2, -2) (a) and symmetry-broken LL ν_{LL}=-2 originated from CNP (b). The inset figures show fitted thermal activation gap according to Arrhenius formula $R \propto \exp(-\Delta/2kT)$.

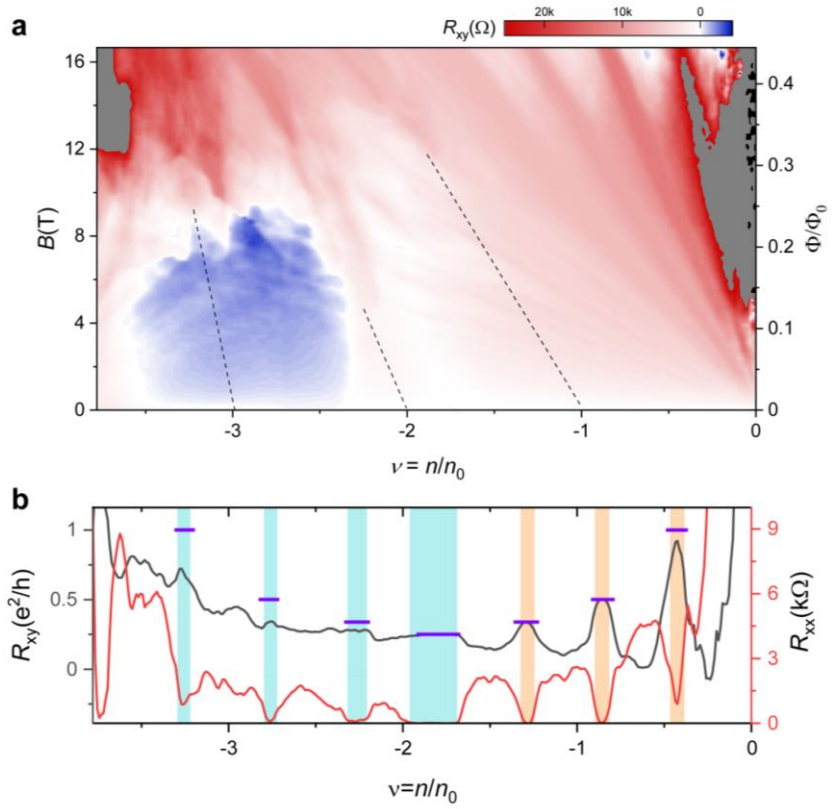

FIG.S5 Hall resistance R_{xy} behaviors in θ=1.25 ° TBG. a, two-dimensional mapping of R_{xy} as a function of carrier density and magnetic fields. Dash lines show expected trajectories of Hall plateaus and R_{xx} minima for Chern insulators. b, line cuts of R_{xy} and R_{xx} at B=16.66T. We mark the Chern insulators (-1, -3), (-2, -2), (-3, -1) and (-4, 0) with light blue shades and symmetry-broken LLs from CNP with orange shades. Additionally, violet bars are added to show the expected quantized value of R_{xy}. All the data are acquired at T=20mK.

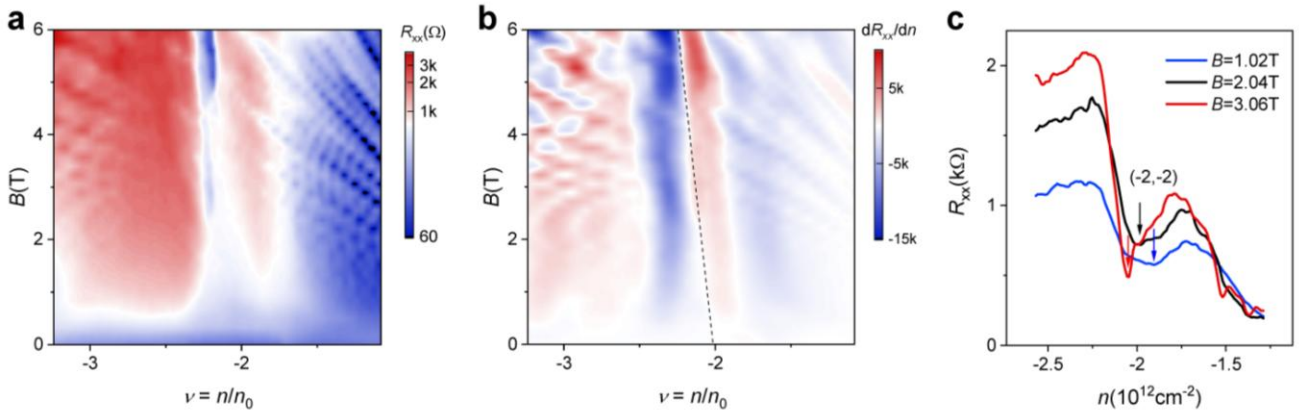

FIG.S6 Onset of Chern insulator (-2, -2) in tiny magnetic fields for θ=1.25 ° TBG. a, zoomed-in Landau fan diagram. b, derivate of R_{xx} with respect to carrier density n as a function of filling ν and field B. c, line cuts of R_{xx} with respect to carrier density. All the data are acquired at T=20mK.

4. Landan fan diagram for varied twist angle

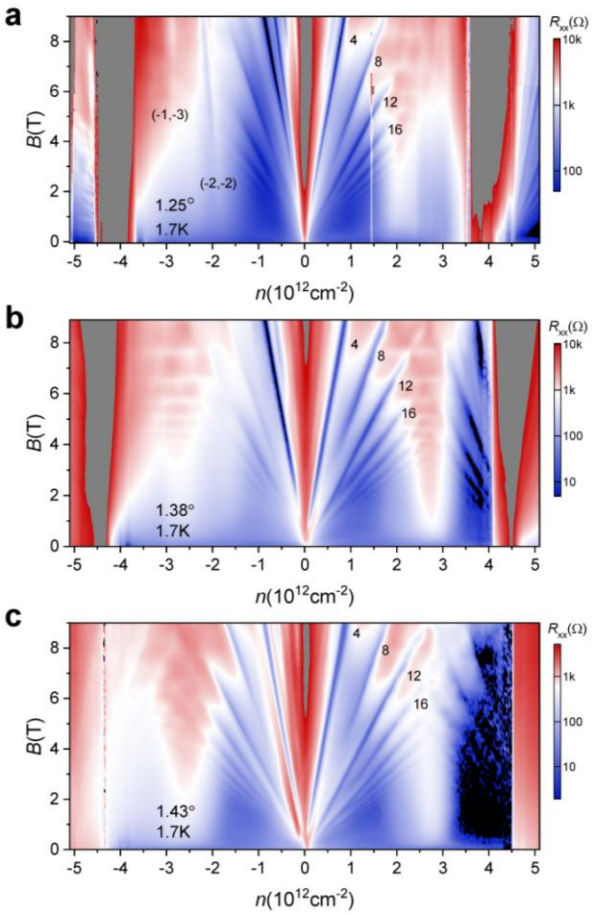

FIG.S7 Landau fan diagram for both of hole and electron branches. The spike line in (a) comes from an unexpected error in our measurement system.

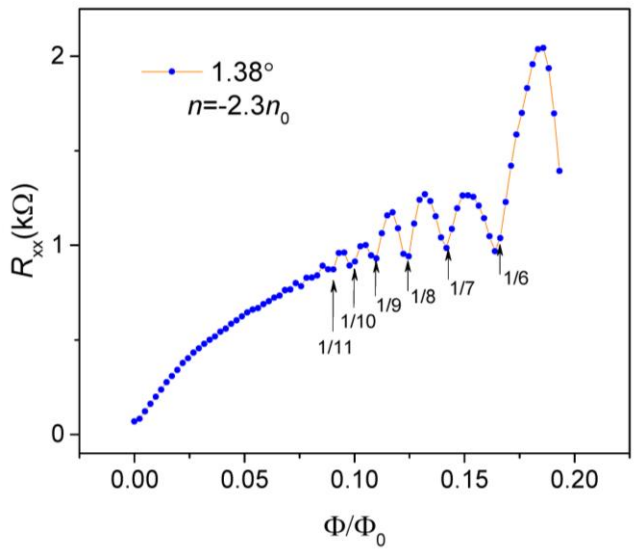

FIG.S8 Brown-Zak oscillation in θ=1.38 ° TBG. The data are obtained from Fig.S7b, shown as a line cut at density n=-2.3n_0.

We show a full image of Landau fan diagram both for electron and hole sides. At T=1.7K and B<9T, Chern insulators (-1, -3) and (-2, -2) still survive in the θ=1.25 ° TBG. We observed more pronounced Brown-Zak oscillations at electron side as compared to one at T=20mK. This behavior is similar to that in graphene/hBN superlattice, where the fractal minibands will evolve into Brown-Zak subbands when temperature is elevated. Fig. S8 shows clearly Brown-Zak oscillations surviving down to ϕ_0/11 in 1.38 °TBG at hole side. While for 1.43 °TBG, no signal of Brown-Zak oscillations is found.

5. Coulomb interaction and kinetic energy

A rigid calculation for Chern band formation at varied twist angle with e-e interaction involved is far beyond the content of our paper, instead we present a general analysis considering the competition between Coulomb interaction and kinetic energy here. In TBG with a small twist angle of θ, the Coulomb interaction can be estimated as $U = \frac{e^2}{4\pi\epsilon\epsilon_0\lambda}$, where e is the electron charge, ϵ the relative dielectric constant, ϵ_0 the vacuum permittivity, and $\lambda \approx \frac{a}{\theta}$ the moire wavelength and *a* the graphene lattice constant. We calculated the Coulomb interaction by assuming ϵ=4 as shown in the picture below. From the continuum model, we extract bandwidth W for valence and conduction band to describe the kinetic energy. The bandwidth of valance band and conduction band is calculated by continuum model. We choose the minimum and maximum points on the path of mini-Brillouin zone from Gamma to M to K to calculate the bandwidth. Therefore, the bandwidth may slightly different from that calculated from the density of the state diagram. The calculation result indicates a crossover at $\theta = 1.27^o$ when U/W=1, which locates the similar range of twist angle where we observed the symmetry-broken Chern insulators.

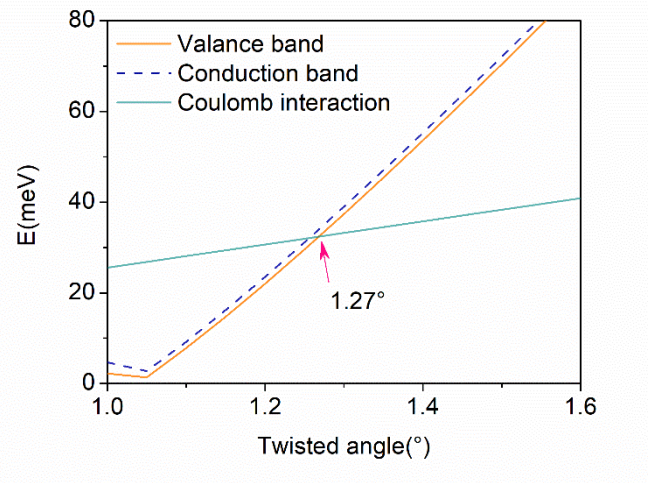

FIG.S9 Band width calculated from continuum model and Coulomb repulsion energy for a small twist angle

It is also noted that the dielectric environments have a strong influence on the Coulomb energy. In our analysis, we chose a relative dielectric constant of 4, which is very close to that of hBN. The agreement between this simple assumption and our experimental results points to a screening effect in 3 dimensions by the dielectric environment. In experiments, ϵ might vary from device to device and bring a big uncertainty when quantifying Coulomb energy.

6. References

1. K. Kim, M. Yankowitz, B. Fallahazad, S. Kang, H. C. P. Movva, S. Huang, S. Larentis, C. M. Corbet, T. Taniguchi, K. Watanabe, S. K. Banerjee, B. J. LeRoy, and E. Tutuc, Van der Waals heterostructures with high accuracy rotational alignment. *Nano. Lett.* **16**, 1989−1995(2016).
2. L. Wang, I. Meric, P. Y. Huang, Q. Gao, Y. Gao, H. Tran, T. Taniguchi, K. Watanabe, L. M. Campos, D. A. Muller, J. Guo, P. Kim, J. Hone, K. L. Shepard, C. R. Dean. One-dimensional electrical contact to a two-dimensional material. *Science* **342,** 614–617 (2013).
3. H. C. Po, L. Zou, A. Vishwanath, and T. Senthil, Origin of Mott insulating behavior and superconductivity in twisted bilayer graphene, *Phys. Rev. X* **8**, 031089 (2018).
4. Y.-H. Zhang, H. C. Po, and T. Senthil, Landau level degeneracy in twisted bilayer graphene: Role of symmetry breaking, *Phys. Rev. B* **100**, 125104 (2019).